Model-less hybrid position/force control: a minimalist approach for continuum manipulators in unknown, constrained environments

Michael C. Yip[1] and David B. Camarillo[2]

***Abstract*—Continuum manipulators are designed to operate in constrained environments that are often unknown or unsensed, relying on body compliance to conform to obstacles. The interaction mechanics between the compliant body and unknown environment present significant challenges for traditional robot control techniques based on modeling these interactions exactly. In this paper, we describe a hybrid position/force control method that uses a model-less approach. Model-less control is a recently-described approach to control that learns the continuum manipulator Jacobian and adapts to constraints in the environment in a safe manner. When interacting with the environment using the end-effector, these tip-constraints can affect the manipulator Jacobian estimates to become ill-conditioned. This paper addresses this issue by defining a hybrid control approach for simultaneously controlling end-effector position and forces while still maintaining the minimalist approach of model-less control. Under this method, continuum manipulators can safely and effectively interact with the environment, even when these interactions are arbitrary and unknown constraints.**

***Index Terms*—Model-less control, hybrid control, position/force control, continuum manipulator, soft robotics.**

I. Introduction

CONTINUUM manipulators offer a unique ability to safely operate within cluttered and constrained environments [1]. Their continuously flexible backbones naturally conform to environmental obstacles. This allows them to move further into a constrained environment as well as passively minimize their interaction forces with the environment, which has been particularly useful and important for medical applications [2]. These medical applications are enabled specifically by the flexibility of continuum manipulators, as rigid-link manipulators would otherwise apply too much force on the tissues and would be unsafe.

One of the key modeling/control differences between rigid-link and continuum manipulators is that interactions with the environment affect the kinematics and mechanics of continuum manipulators in an unknown manner (Fig. 1). Specifically, because of the continuously flexible nature of their backbones, their configurations are rarely sensed completely, nor are environmental interactions that affect the robot configuration.

Manuscript received: August 31, 2015; Accepted January 16, 2016.

This paper was recommended for publication by Editor Kevin Lynch upon evaluation of the Associate Editor and Reviewers' comments.

[1]Michael C. Yip is with the Electrical and Computer Engineering Department, University of California San Diego, USA. yip@ucsd.edu

[2]David B. Camarillo is with the Department of Bioengineering, Stanford University, USA. dcamarillo@stanford.edu

Digital Object Identifier (DOI): see top of this page.

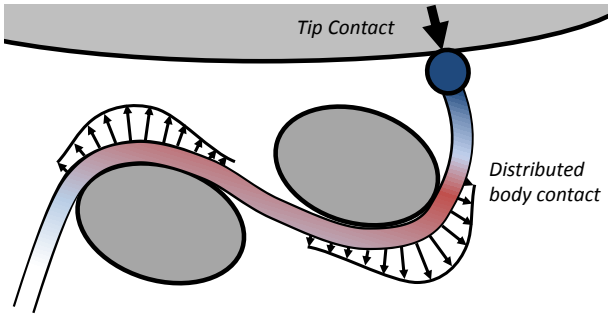

Fig. 1. A continuum manipulator routinely interacts with constrained environments in unknown and uncontrollable ways.

This makes the mathematical modeling of continuum manipulators very tricky. We have recently demonstrated a *model-less control* method that does not use a kinematics or mechanics model of the manipulator [3]. The model-less control estimates the robot Jacobian in real-time using measurements of the actuator and the position of the tip, and feeding back the estimate for closed-loop task-space control.

The original model-less control method works well when the robot is constrained by unknown obstacles on its body, where it will naturally conform to the environment. However, some challenges still persist. First, interaction forces with environments at the continuum manipulator end-effector (tip) are not currently regulated, suggesting that a force-control approach be used, and only a small number of model-based methods have been described for continuum manipulators [4], [5]. The second challenge is more subtle but of significance to model-less control: when a manipulator tip comes into contact with an obstacle, it experiences a velocity discontinuity. For a hard contact, motion into contact will become zero. On a continuum manipulator, the actuation drives a degree-of-freedom in the bending of the body, while appearing to have a muted effect on tip motion in one direction. This results in a poorly-conditioned Jacobian estimate using model-less control. For stiff contacts, the condition of the Jacobian will be near singularity, and will cause the actuators to ramp up significantly and drive much harder to maintain position and rate tracking.

In this paper, we present a novel hybrid position/force control method for constrained manipulators with unknown mechanics and kinematics. Furthermore, constraints on the manipulator body's configuration are also unknown. Compared to prior work, this new model-less hybrid control can be

applied to a spectrum of continuum manipulators with varying bending mechanics/kinematics that may not be well understood, and where limited sensing (robot or environment) is available.

II. Prior Work

Traditional robotic control techniques rely on an accurate model of the manipulator in order to solve for joint displacements and torques. Because the environment can conform continuum manipulators into irregular and unpredictable configurations, modeling of continuum manipulators is a challenging endeavor. Models describing manipulator kinematics have been formulated for tendon-driven manipulators [6]–[8], pneumatically/hydraulically actuated manipulators [9], concentric-tube manipulators [10]–[13], and SMA-actuated manipulators. These kinematic models assume geometric configurations such as constant-curvature or elliptical bending that can be inexact [14]. Mechanics models have been developed for tendon-driven manipulators [15], pneumatically/hydraulically actuated manipulators [9], [16]–[18], for concentric-tube manipulators [12], [19], [20], and for SMA-actuated manipulators [21]–[24]. The mechanics of the continuum manipulators are influenced by unidealities in the actuation mechanisms, such as sliding frictions within tendon-driven manipulators, and these have recently been investigated as well [20], [25].

The difficulty with modeling continuum backbones is that two effects must be captured in the model: the robot's unidealities (e.g. internal drive friction, hysteresis, backlash) and environmental effects on configuration. Some work has been done to achieve full configuration sensing [26]–[30], but require either camera line-of-sight or fiber-bragg gratings that cannot conform significantly without wear, are sensitive and costly to implement.

All the methods presented so far have relied on the passive compliance of continuum manipulators to enable safe navigation. Hybrid control of position and forces provide a means of active compliance [31]. These controllers rely on models of the manipulator Jacobian from kinematic and mechanics to perform closed-loop control, and have recently been used to regulate forces and estimate environmental stiffnesses in continuum manipulators [4], [23], [32]. These methods regulated tip forces of manipulators under well-understood conformation (i.e. free-space motion). Most recently, Bajo et al. [5] demonstrated intrinsic sensing and control of forces interacting with the manipulator body. So far, these methods have relied on in-depth characterization and calibration to complex mechanics models, as well as multiple configuration sensors to identify object interactions with the robot.

III. Methods

In model-less control, we will estimate the Jacobian matrix in real-time to take into account the effects of unmodelled environmental effects and robot unidealities. The control method comprises two components: a closed-loop optimal controller that solves for actuator displacements, and a Jacobian estimation method that continuously learns a local Jacobian estimate online while traversing the environment. The methods described below are generalized for an m degree-of-freedom robot in three-dimensional (3D) space. The full control loop is shown in Fig. 2.

(1) Initialization:
Let $\mathbf{x} = [x_1 ... x_n]^\top$ represent the tip pose of the robot and $\mathbf{y} = [y_1 ... y_m]^\top$ represent actuator positions. A Jacobian matrix $\mathbf{J}$ is initialized by moving each actuator independently an incremental amount, Δy_i while measuring the displacement $\Delta\mathbf{x}$. The ith column of $\mathbf{J}$ is constructed as $\mathbf{J_i} = \Delta\mathbf{x}/\Delta y_i$, such that

$$\mathbf{J} = [\mathbf{J_1} \cdots \mathbf{J_n}]. \tag{1}$$

A weighting matrix $\mathbf{W}$ is constructed to normalize the actuator signals, such that

$$\mathbf{W} = \text{diag}\left(||\mathbf{J_1}||_2, \cdots, ||\mathbf{J_n}||_2\right), \tag{2}$$

where $||\cdot||_2$ is the vector 2-norm operator. Then,

$$\Delta\mathbf{x} = \hat{\mathbf{J}}\mathbf{W}\Delta\mathbf{y}. \tag{3}$$

where $\hat{\mathbf{J}} = \mathbf{J}\mathbf{W}^{-1}$ is the Jacobian matrix estimate with column vectors of unit length. $\mathbf{W}\Delta\mathbf{y}$ scales the actuator signals such that, when solving for actuator displacements using a least-norm optimization method described later, the actuators are equally weighted.

Tendon-driven continuum manipulators are often redundantly actuated in order to achieve omni-directional actuation [8]. In these cases, co-activation of tendons results in pretensions along the tendons and the body of the manipulator — a quantity of interest that can be minimized to avoid buckling. Tendon tensions can be related to tendon displacements by a linear function [15], so we define a diagonal stiffness matrix $\mathbf{K}_\tau$, such that:

$$\Delta\tau = \mathbf{K}_\tau\Delta\mathbf{y}, \tag{4}$$

where τ is the tension in the tendons. Columns of $\mathbf{K}_\tau$ can be constructed by moving each actuator separately and measuring the change in tensions in all tendons. Tendon tensions τ are measured using a load cell for each tendon.

(2) Contact Estimation:
Contact estimation is performed through a force sensor. The force sensor reads a tri-axial force measurement; these forces are measured in the manipulator frame $\{C_m\}$ (Fig. 2). These forces are then defined in the environment frame $\{C_e\}$ (the same frame in which the desired reference position and reference forces are described) using the rotation matrix ${}^e_m\mathbf{R}$. Let $\mathbf{F} = {}^e_m\mathbf{R}\mathbf{F}_{\text{sensor}}$ be the forces already defined in the environment frame; the direction of the contact force is then $u_\mathbf{F} = \mathbf{F}/||\mathbf{F}||_2$ where $||\cdot||_2$ is the vector 2-norm operator. The underlying assumption here is that Coulomb friction does not significantly change the surface normal measured at the tip of the manipulator (e.g. operating within the lubricated anatomy of the body) and where sharp corners or deep indentations in the environment are not encountered.

Forces along $u_\mathbf{F}$ are the controlled variable, and displacement in the direction in the plane orthogonal to $u_\mathbf{F}$ are the controlled variable [31]. Positions in the $u_\mathbf{F}$ direction

This article has been accepted for publication in a future issue of this journal, but has not been fully edited. Content may change prior to final publication. Citation information: DOI 10.1109/LRA.2016.2526062, IEEE Robotics and Automation Letters

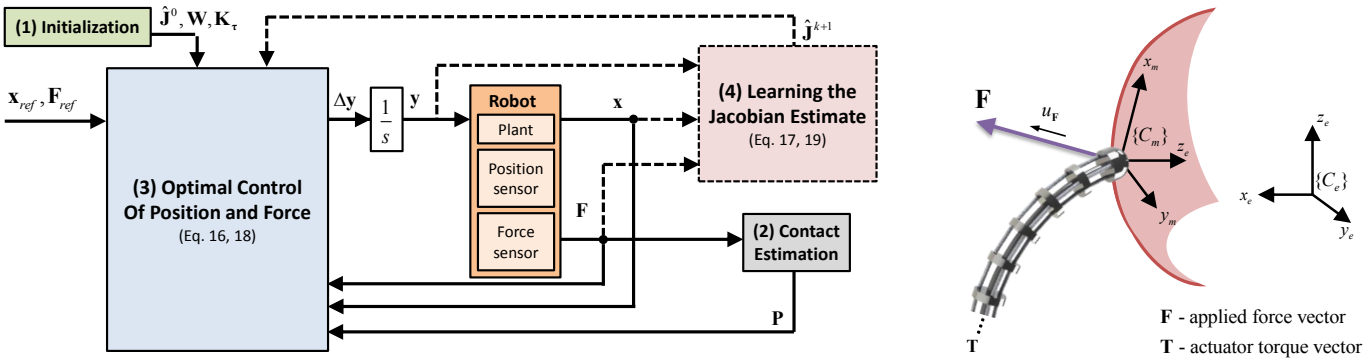

Fig. 2. The full closed-loop controller. Solid lines show the portion of the controller that controls the manipulator actuation, while dashed lines show the portion of the controller that continuously learns the Jacobian estimate. The manipulator and environment interaction is shown on the right.

are assumed to not be directly controllable; forces in the plane orthogonal are also not controlled and furthermore are assumed to be zero given our assumption of local-planar contact. This will be useful for avoiding trying to regulate forces and positions in the uncontrollable directions.

(3) Optimal Control of Position and Force:
The optimal closed-loop controller shown in Fig. 2 minimizes a combination of objectives given a number of physical constraints. Closed-loop control of the unconstrained direction is done through (3) as

$$\Delta\mathbf{x} = \hat{\mathbf{J}}\mathbf{W}\Delta\mathbf{y}_\mathbf{x} \tag{5}$$

where $\Delta\mathbf{y}_\mathbf{x}$ is the actuation responsible for moving the manipulator in the unconstrained direction. Let $\Delta\mathbf{x}$ describe a desired displacement in an unconstrained direction. Given a proportional gain closed-loop controller, the desired displacement is described as

$$\Delta\mathbf{x} = \begin{cases} \mathbf{K}_\mathbf{x}(\mathbf{I}-\mathbf{P})(\mathbf{x}_{\text{ref}}-\mathbf{x}) & \text{if } u_\mathbf{F}^\top\Delta\mathbf{x} < 0, \\ \mathbf{K}_\mathbf{x}(\mathbf{x}_{\text{ref}}-\mathbf{x}) & \text{otherwise.} \end{cases} \tag{6}$$

where $\mathbf{x}_{\text{ref}}$ is the reference trajectory, $\mathbf{x}$ is the measured position, and $\mathbf{K}_\mathbf{x}$ is the proportional gain. $\mathbf{P} = \mathbf{u}_\mathbf{F}\mathbf{u}_\mathbf{F}^\top$ is a projection into the contact normal, and $\mathbf{I}-\mathbf{P}$ is a projection onto the unconstrained plane. This definition avoids controlling positions when moving into the surface, but allows the user to define positions that move the manipulator off-contact. Similarly, the desired change in force using a proportional gain closed-loop controller is described as

$$\Delta\mathbf{F} = \mathbf{K}_\mathbf{F}\mathbf{P}(\mathbf{F}_{\text{ref}}-\mathbf{F}), \tag{7}$$

where $\mathbf{F}_{\text{ref}}$ is the reference force, $\mathbf{F}$ is the measured force, and $\mathbf{K}_\mathbf{F}$ is the proportional gain.

Consider a force constraint as a simple linear spring approximation of the continuum manipulator's backbone and an environment with a certain stiffness, which when in contact act as a series-elastic system [4]. For a series-elastic system, the difference between the measured position $\mathbf{x}$ and its unconstrained (rest) location x' presents a spring force from the compression of the manipulator; similarly, the difference $\mathbf{x}$ and the unconstrained contact location $\mathbf{x_0}$ presents an opposing force from the environment. These are described below as

$$\begin{aligned} \mathbf{F}_m &= \mathbf{K}_m(\mathbf{x}-\mathbf{x}') \\ \mathbf{F}_e &= \mathbf{K}_e(\mathbf{x}-\mathbf{x}_0) \end{aligned} \tag{8}$$

where $\mathbf{K}_m$ and $\mathbf{K}_e$ are the manipulator stiffness and environmental stiffness matrices respectively, and are non-negative and symmetric. These measurements can either be measured a-priori or estimated, and do not need to be especially accurate since the proportional gains $\mathbf{K_F}$ act as a gain to the stiffness estimates in the closed-loop controller. This series-elastic system results in a relationship between force and displacement

$$\Delta\mathbf{F}_m = -\Delta\mathbf{F}_e = \mathbf{K}_r\Delta\mathbf{x} \tag{9}$$

where $\mathbf{K}_r = \mathbf{K}_e\mathbf{K}_m(\mathbf{K}_e+\mathbf{K}_m)^{-1}$ is the resultant stiffness mapping between the actuated displacement and the output force of the manipulator, and is non-negative and symmetric. Then, from (3) and (8), a desired change in force $\Delta\mathbf{F}$ is described by

$$\Delta\mathbf{F} = \mathbf{K}_r\hat{\mathbf{J}}\mathbf{W}\Delta\mathbf{y}_\mathbf{F}. \tag{10}$$

where $\Delta\mathbf{y}_\mathbf{F}$ is the actuation responsible for applying forces in the direction of contact, and therefore we have

$$(\mathbf{I}-\mathbf{P})\hat{\mathbf{J}}\mathbf{W}\Delta\mathbf{y}_\mathbf{F} = 0. \tag{11}$$

Finally, for a tendon-driven manipulator, the controller should ensure that tendons maintain a positive tension so that they do not go slack. Thus, to maintain a constant positive tension and using (4),

$$\tau + \Delta\tau \succeq \epsilon. \tag{12}$$

The complete closed-loop controller, where (6) and (7) together form the proportional position/force control law, is

$$\begin{aligned} \underset{\Delta\mathbf{y}}{\text{minimize}} \quad & \sum_{i=1}^{3}\lambda_i||h_i||_2 \\ h_i = \begin{cases} h_1 = \Delta\mathbf{y}_\mathbf{F} \\ h_2 = \Delta\mathbf{y}_\mathbf{x} \\ h_3 = \tau+\Delta\tau \end{cases} \end{aligned} \tag{13}$$

This article has been accepted for publication in a future issue of this journal, but has not been fully edited. Content may change prior to final publication. Citation information: DOI 10.1109/LRA.2016.2526062, IEEE Robotics and Automation Letters

subject to

$$\Delta\mathbf{x} = \hat{\mathbf{J}}\mathbf{W}\Delta\mathbf{y_x}$$
$$\Delta\mathbf{F} = \mathbf{K}_r\hat{\mathbf{J}}\mathbf{W}\Delta\mathbf{y_F}$$
$$\tau + \Delta\tau \succeq \epsilon,\ \Delta\tau = \mathbf{K}_\tau\Delta\mathbf{y}$$
$$\Delta\mathbf{y} = \Delta\mathbf{y_x} + \Delta\mathbf{y_F}$$

The L2-norm of the objective functions $||h_i||_2, i = 1..3$ with weightings $\lambda_i, i = 1..3$ is used to find the pareto-optimal least-squares solution for actuator displacements $\Delta\mathbf{y}$. This is chosen because it will (i) minimize actuation for regulating force, and (ii) minimize actuation for following a trajectory, and (iii) minimize the total tendon tensions of the system and limit axial compression. λ is chosen so that range of actuation and tension are equally weighted, but can also be chosen to weight different objectives differently. $\Delta\mathbf{y_x}$ and $\Delta\mathbf{y_F}$ are explicitly minimized as they independently control positioning and force-reflecting actuations. Although the position and force constraints are orthogonal, the solution space for $\Delta\mathbf{y_x}$, $\Delta\mathbf{y_F}$ are not orthogonal. Thus, if minimizing only their sum, $\Delta\mathbf{y}$, we lose independent control of position and force actuations. A discussion of the system stability is provided in the Appendix. When the tip is not measuring contact with the environment, then force control is turned off and effectively becomes the model-less controller in [3]. This can be done by setting $\mathbf{P} = \mathbf{0}$ when $||\mathbf{F}||_2 \approx 0$.

(4) Learning the Jacobian Estimate:

The model-less control method [3] works well when the robot is constrained by unknown obstacles on its body. We modify the method here to update the Jacobian estimate with consideration of the contact by solving the following constrained optimization problem

$$\begin{aligned} \underset{\hat{\mathbf{J}}^{\mathbf{k+1}}}{\text{minimize}} \quad & ||\Delta\hat{\mathbf{J}}||_2 \\ \text{subject to} \quad & (\mathbf{I}-\mathbf{P})\Delta\mathbf{x} = (\mathbf{I}-\mathbf{P})\hat{\mathbf{J}}^{k+1}\mathbf{W}\Delta\mathbf{y} \\ & \hat{\mathbf{J}}^{k+1} = \hat{\mathbf{J}}^{k} + \Delta\hat{\mathbf{J}} \end{aligned} \tag{14}$$

where $\Delta\mathbf{x}$ is the measured end-effector displacement when it is constrained, and $\Delta\mathbf{y}$ is the change in actuation, and $(\mathbf{I}-\mathbf{P})$ is used to mask the force-reflecting direction from the Jacobian estimate where $\mathbf{I}$ is the identity. Thus, the Jacobian estimate combines prior estimates from the force-reflecting direction with the new estimates in the measured, non-force-reflecting directions to stay updated. Here, $||\Delta\hat{\mathbf{J}}||_2$ represents the Frobenius norm of the estimation update matrix $\Delta\hat{\mathbf{J}}$. Minimizing the Frobenius norm was chosen as a way to have the Jacobian estimate change at small increments between timesteps resulting in smoother controller actuations.

IV. Experiments and Results

A. Experimental Setup

The proposed controller was implemented on a tendon-driven continuum manipulator (Fig. 3) comprising a flexible backbone (length: 280 mm, cross-section: 0.8 mm $\times$12 mm, polypropylene, 37 MPa, McMaster Carr) and two 0.6 mm diameter steel wire tendons. 3D printed plates placed evenly over the length of the backbone act as vertebrae and provide a guide for the tendons to pass through. Two tendons and an insertion actuator drive the catheter in a planar environment. Tendons terminate at tension sensors (LSP-5, range 0-5 kg, Transducer Techniques), which measure cable tensions during tendon actuation; the tension sensors (and therefore the tendons) are pulled using individual servo gear-motors. An insertion motor drives the robot forwards and backwards. Tri-axial forces at the manipulator tip are measured with a force transducer (Nano17, ATI Industrial Automation) with a 3 mN resolution. A single, uncalibrated camera (Playstation Eye, 480×640 pixels, Sony Entertainment Corporation) is placed 50 cm above the environment facing downwards, providing position tracking at 50 Hz at a resolution of approximately 0.5 mm per pixel. The position of two optical markers provide position and orientation at the tip.

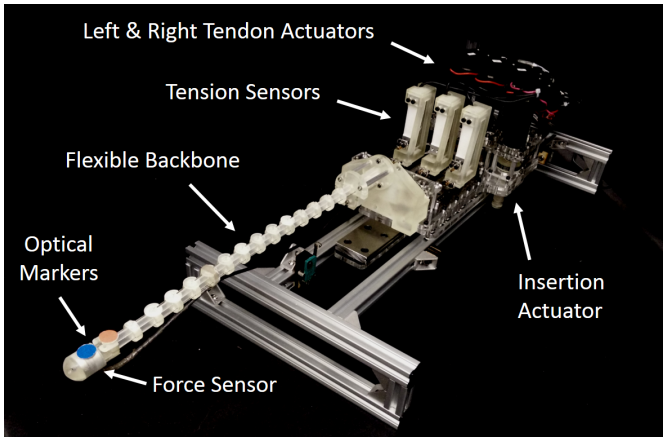

Fig. 3. A continuum manipulator with an antagonistic tendon drive and insertion actuator. Force sensing is achieved using a distal force sensor, and tendon tensions are measured using proximal load cells. An overhead camera (not shown) provides 2D tracking in the workspace.

To minimize the effects of digitization, Jacobian estimations were run when the manipulator had moved more than 8 pixels (4 mm). We also apply a smoothing term to the Jacobian estimate of $\hat{\mathbf{J}}^{k+1} = \hat{\mathbf{J}}^{k} + \alpha\Delta\hat{\mathbf{J}}$, $\alpha = 0.5$; this was chosen experimentally and simply done for practical purposes to minimize effects of noisy sensor data readings. The proportional controller gains were tuned to achieve a damped response. A minimum tendon tension of $\tau = 0.3$ N was maintained using the constrained optimization method during each control cycle.

To calculate $\mathbf{K}_r$, we approximated the manipulator stiffness with a simple diagonal stiffness map with axial stiffness K_a, and bending stiffness K_b, such that $\mathbf{K}_r = \mathbf{K}_e\mathbf{K}_m(\mathbf{K}_e + \mathbf{K}_m)^{-1}$, and $\mathbf{K}_m = {}^e_m\mathbf{R}\text{diag}(K_a, K_b, K_b){}^e_m\mathbf{R}^\top$. We empirically set the axial stiffness to 0.1 N/mm and a bending stiffness to 0.01 N/mm to better reflect the reality that the continuum manipulator is anisotropically stiff.

The optimal closed-loop control and the Jacobian estimation optimizations were performed using the CVXgen convex optimization solver [33]. The closed-loop computation time was below 500 μsec.

This article has been accepted for publication in a future issue of this journal, but has not been fully edited. Content may change prior to final publication. Citation information: DOI 10.1109/LRA.2016.2526062, IEEE Robotics and Automation Letters

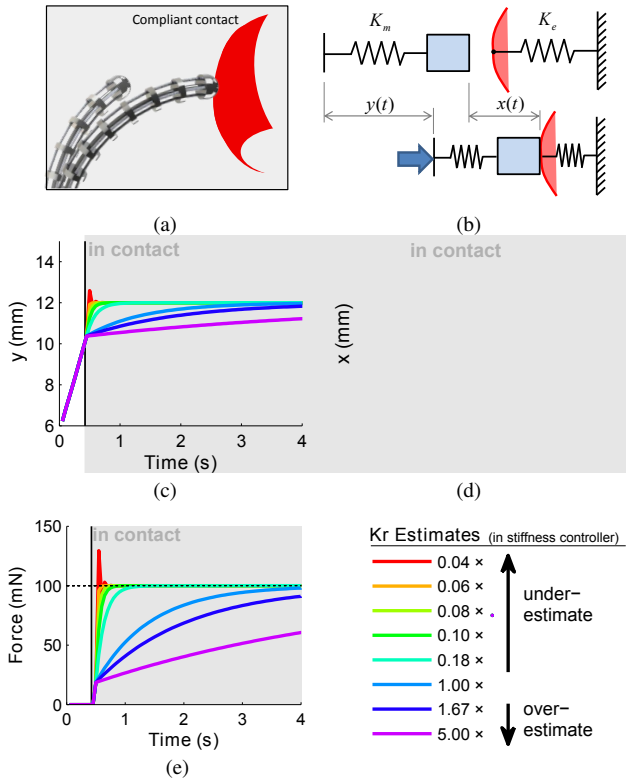

Fig. 4. A manipulator (a) comes into contact with a wall (b). For hybrid control, we demonstrate the effect of overestimating and underestimating K_r in (13), between 4% to 500% of the actual stiffness. (c) shows the actuation y of a tendon to achieve a position/force trajectory, (d) shows the regulated position x, (e) shows the regulated force.

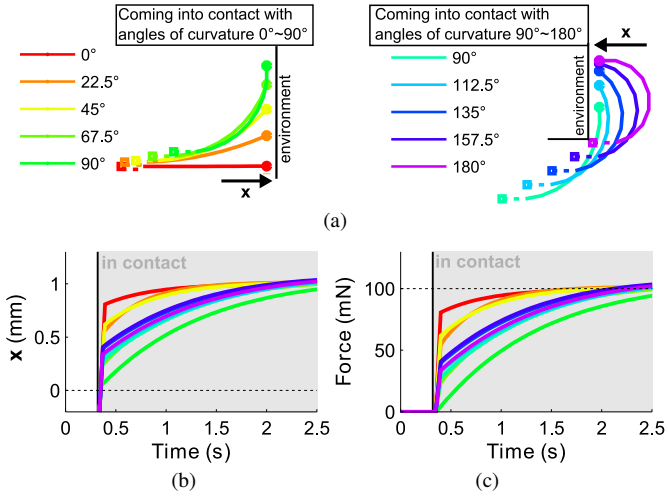

Fig. 5. We examined the anisotropic effect of the manipulator on the hybrid controller. (a) shows the configuration in which the manipulator comes in contact with the environment at different angles, (b) shows the regulated displacement in a compliant environment, and (c) shows the regulated force. The controller remains stable in these conditions.

B. Simulation of model-less hybrid control

We first investigate the controller performance in different contact environments and approaches using a simulated robot. Fig. 4 shows the simultaneous control of position and force exerted on an environment with a stiffness $K_r = 0.05$ N/mm.

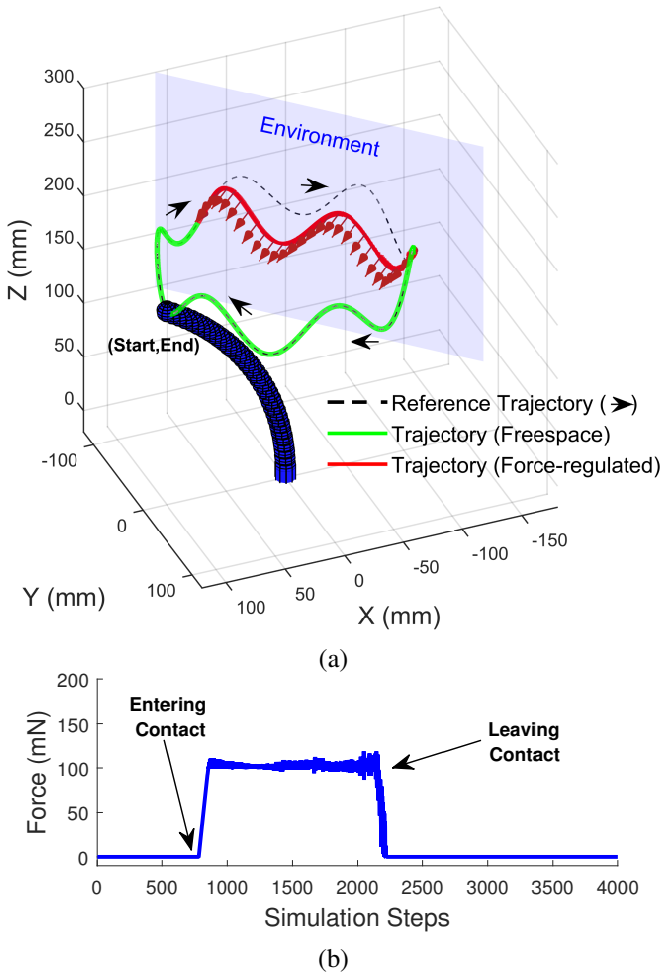

Fig. 6. (a) Simulation of a position/force regulated task where the manipulator enters contact with an unknown, stiff environment. The robot is able to regulate forces with the environment to within a desired range of contact (b), and is able to come off the environment and continue in position control. These are done while continuously estimated the robot Jacobian.

By controlling forces, we successfully mitigate actuator wind-up, allowing the robot to avoid internal loading and buckling. We also show the effect of error in the estimated K_r. Under-damped motion occurs when $K_r = 0.05$ is underestimated by nearly two orders of magnitude, or 50 times softer than the actual environment. Otherwise, the manipulator provides an overdamped, smooth response. Furthermore, modifying K_F tunes the controller to be more conservative or more aggressive in its regulation of manipulator forces.

We also investigated the anisotropic stiffness of the continuum manipulators, having different axial and bending compliance (Fig. 5), and its empirical effect on controller performance. The manipulator is asked to enter into contact with a stiff environment $K_e = 0.1$ N/mm and maintain contact. The manipulator has an axial stiffness of 1.0 N/mm and bending stiffness of 0.1 N/mm. The controller is able to both maintain constant and stable contact with the environment, under various curvatures and interaction stiffnesses with the environment.

An example scenario is shown in Figure 6, where a continuum manipulator is operating in 3D space. The manipulator,

This article has been accepted for publication in a future issue of this journal, but has not been fully edited. Content may change prior to final publication. Citation information: DOI 10.1109/LRA.2016.2526062, IEEE Robotics and Automation Letters

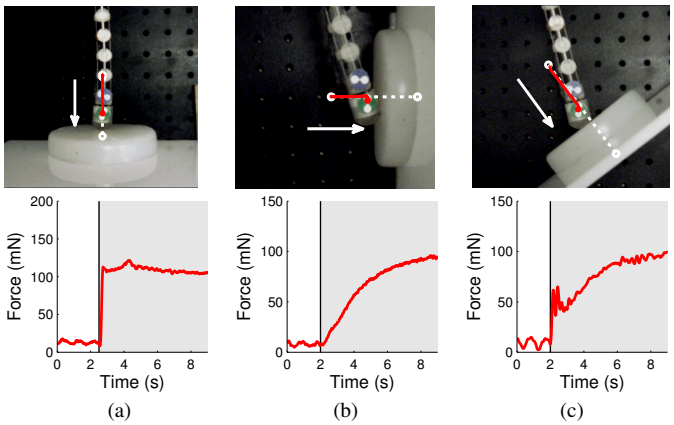

Fig. 7. The manipulator moves into the environment at different angles, requiring different actuation torques and along varying axes of manipulator stiffness ($\mathbf{K}_m$): insertion actuation in the axial direction (a), tendon actuation in the transverse direction (b), and insertion and tendon actuation in the diagonal direction (c).

with backbone stiffness defined from [15], is configured with 3 tendon actuators drive the 360° bending of the continuum manipulator [8], and an insert/retract actuator drives the robot into and out of the environment. The manipulator follows a varying position trajectory, but comes into contact with an unknown stiff wall and continues to follow the intended trajectory while regulating forces.

C. Physical experiments of canonical contact scenarios

The most effective method for evaluating our method is in a physical setup. A position trajectory was tracked while controlling the desired interaction forces for different contact scenarios in Fig. 7. The continuum manipulator began in freespace, and it followed a trajectory that introduces its end-effector into an environmental constraint. The controller was asked to maintain 100 mN of force when in contact with the environment. Here, three canonical cases are demonstrated, showing the manipulator interacting with the environment in its axial direction (Fig. 7a), its transverse directions (Fig. 7b) and in a combined, diagonal direction (Fig. 7c). This is to vary the combination of actuators required for position/force.

The transition from freespace to a constrained configuration is shown to be stable. Forces converge to the desired level without any notable oscillatory behavior. At contact, the Jacobian matrix is appropriately updated and successfully avoids actuator wind-up caused by a contact singularity. Differences in the speed of convergence to the desired forces can be attributed to differences in axial and bending stiffnesses of the manipulator.

D. Position/force control in a complex contact scenario

Fig. 8 demonstrates the continuum manipulator moving through a series of constraints, resulting in complex contact scenarios and unpredictable conformations. The trajectory it follows moves the manipulator into a body-constraint followed by a tip-constraint simultaneously; the manipulator is then asked to maintain a constant force (80 mN) along a wall

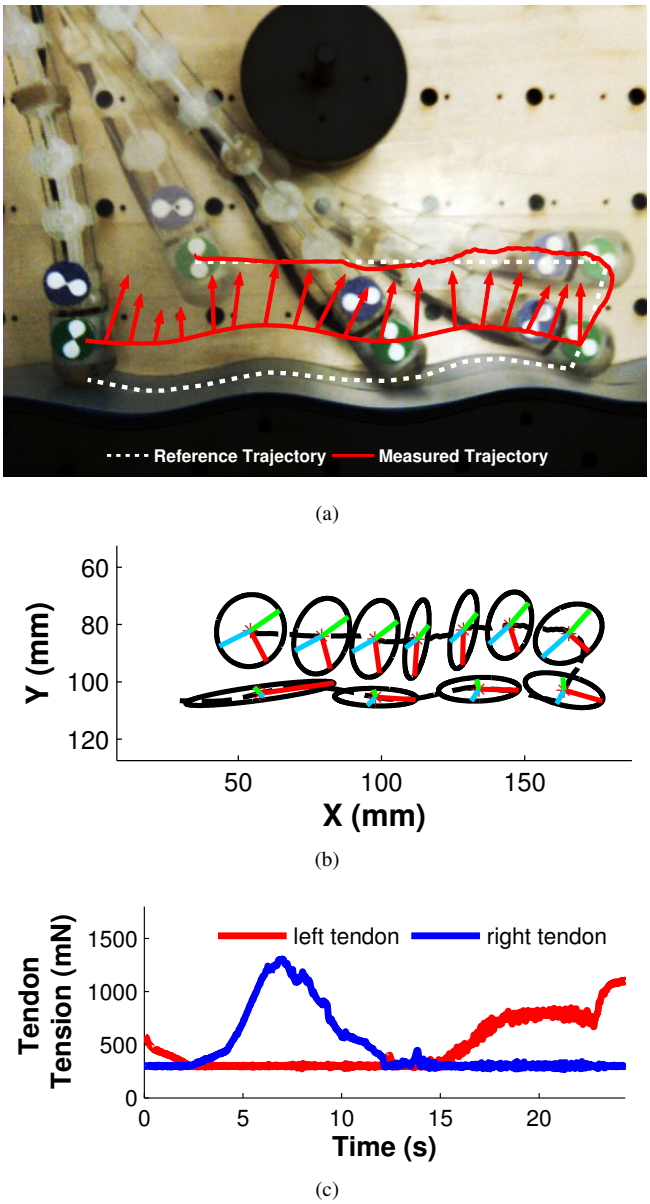

Fig. 8. The robot moves through an unknown, complex environment with varying body and tip constraints. (a) the controller regulates a constant 80 mN force (arrows) when it senses the waving surface contact. (b) shows Jacobian estimates of the robot as ellipses [34, pg. 236], and (c) shows that tendon tensions are minimized while remaining taut.

that has fluctuating surface normals and depth. The controller allows the manipulator to regulate positions/forces properly even under unknown body- and tip-constraints, while selectively updating the Jacobian matrices throughout the trajectory (Fig. 8b). The controller is able to maintain the 80 mN force with the environment while tracing the non-linear surface under multiple constraints (Fig. 8c). This demonstrates the capabilities of the controller and its ability to adapt to the environment in a stable manner.

E. A touch-and-drag task for medical catheter applications

One promising medical application for continuum manipulators is for controlling ablation catheters. In order to perform a

This article has been accepted for publication in a future issue of this journal, but has not been fully edited. Content may change prior to final publication. Citation information: DOI 10.1109/LRA.2016.2526062, IEEE Robotics and Automation Letters

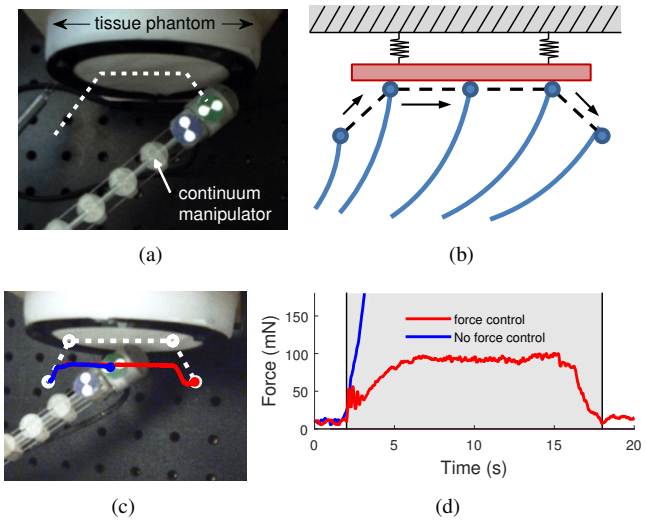

Fig. 9. A robot manipulator (a) coming into tip-contact with a soft constraint and tracing a path along the constraint (b), as is done for cardiac tissue ablation. The (c) tracking accuracy, and (d) interaction forces are shown. A non-force-regulated model-less controller (blue line) fails to perform the task while the proposed controller is able to complete the ablation task under regulated forces.

proper ablation, the catheter needs to apply sufficient pressure at its tip to the tissue in order to achieve cell necrosis, usually through high-intensity radio-frequency energy. Furthermore, contiguous linear ablations are necessary to segregate healthy tissues from erroneous and arrhythmia-inducing electrical signals. Control of these contiguous paths and forces are most effectively done in task-space and therefore it is a good environment for applying the proposed position/force controller. Fig. 9 shows the continuum manipulator applying pressure and tracing a linear path on a silicone tissue phantom with an elastic stiffness of 0.32MPa, emulating the stiffness of a diseased human heart [35]. We are able to trace a user-defined trajectory while applying pressure to the environment. Forces with the soft tissue phantom are regulated to a safe level of approximately 100 mN.

V. Discussion/Conclusion

In this paper, we presented a control solution for addressing the challenges of navigating continuum manipulators in environments where there are unknown body and tip constraints on the robot. We developed a hybrid position/force control approach that can be used to control the manipulator end effector position/force in the presence of unknown body constraints. By continuously learning the robot Jacobian online, we accounted for the effects of unknown environmental constraints on body, and tip-constrained motion and forces. We successfully adapted our Jacobian estimate to account for motions along a variety of environments in which the tip of the robot was constrained. This method thus is an effective and applicable method for continuum manipulators that have complex or unknown bending mechanics, especially when navigating unknown environmental obstacles and constraints.

A number of limitations are known for the proposed method. First, the method relies on sensor accuracy for its estimation method; this is the compromise for not using a model-based controller and instead using a completely data-driven technique for feedback control. As with any control method, and perhaps with more importance to model-less control, sensor resolution and temporal discretization can require heavier signal processing/filtering that introduces estimation lag and limits the performance of the controller. Characterizing the effects of lagging Jacobian estimation is an interesting problem and is subject to future work. Second, a distal force sensor is required. These, however, are now accessible technologies and have commercial use in 3 mm diameter catheters [36]. Third, as with most force-control methods, we presume that the robot is not stuck in a stiff indentation where the force vectors would bounce between two or three directions, and sharp convex edges could also produce a sudden loss of contact so force tracking may be lost or difficult to regulate in these situations. Finally, we use an estimate of manipulator stiffness that should be estimated to within a order of magnitude for the force control, since it can otherwise result in under-damped responses. A potential method is to continuously measuring the environmental stiffness based on the tip-displacements and measured forces in the environment [5]. This presents the more practical aspects of implementing such a controller, which is that without a kinematic or mechanics model of the manipulator, we have an additional tuning parameter in the control system. A combined model-based and our learning-based approach could capture the benefits of both methods and provide optimal performance.

Appendix

Stability: We show that under ideal conditions (no hold effects, delay, etc.) the hybrid position/force control with the model-less Jacobian is stable. We begin with a desired task-space position and force $\{\mathbf{x}_d, \mathbf{F}_d\}$ and the task-space position and force $\{\mathbf{x}, \mathbf{F}\}$. The error is defined as $\mathbf{e_x} = \mathbf{x}_d - \mathbf{x}$ and $\mathbf{e_F} = \mathbf{F}_d - \mathbf{F}$. The change in error is:

$$\dot{\mathbf{e}}_\mathbf{x} = \dot{\mathbf{x}}_d - \dot{\mathbf{x}}. \tag{15}$$

By substituting our real-time Jacobian estimate (3), we have

$$\dot{\mathbf{e}}_\mathbf{x} = \dot{\mathbf{x}}_d - \hat{\mathbf{J}}\mathbf{W}\dot{\mathbf{y}} \tag{16}$$

We define a Lyapunov candidate function

$$V(\mathbf{e}_x) = \frac{1}{2}\mathbf{e}_\mathbf{x}^\top \mathbf{e}_\mathbf{x} \tag{17}$$

Its derivative is defined as

$$\begin{aligned} \dot{V}(\mathbf{e}_x) &= \mathbf{e}_\mathbf{x}^\top \dot{\mathbf{e}}_\mathbf{x} \\ &= \mathbf{e}_\mathbf{x}^\top \dot{\mathbf{x}}_d - \mathbf{e}_\mathbf{x}^\top \hat{\mathbf{J}}\mathbf{W}\dot{\mathbf{y}} \end{aligned} \tag{18}$$

where $\dot{V}(\mathbf{e_x}) < 0$ for asymptotic stability.

We now use the proportional control law (13), where

$$\dot{\mathbf{y}} = \dot{\mathbf{y}}_\mathbf{x} + \dot{\mathbf{y}}_\mathbf{F} \tag{19}$$

such that

$$\dot{V}(\mathbf{e_x}) = \mathbf{e}_\mathbf{x}^\top \dot{\mathbf{x}}_d - \mathbf{e}_\mathbf{x}^\top \hat{\mathbf{J}}\mathbf{W}\dot{\mathbf{y}}_\mathbf{x} - \mathbf{e}_\mathbf{x}^\top \hat{\mathbf{J}}\mathbf{W}\dot{\mathbf{y}}_\mathbf{F} \tag{20}$$

Substituting the orthogonality condition between $\mathbf{e_x}$ and $\hat{\mathbf{J}}\dot{\mathbf{y}}_\mathbf{F}$ from (11), we reduce (20) to be

$$\dot{V}(\mathbf{e_x}) = \mathbf{e_x}^\top \dot{\mathbf{x}}_d - \mathbf{e_x}^\top \hat{\mathbf{J}}\mathbf{W}\dot{\mathbf{y}}_\mathbf{x}. \quad (21)$$

Consider a case where the minimum tendon-tension constraints in (13) are satisfied; then (21) becomes

$$= \mathbf{e_x}^\top \dot{\mathbf{x}}_d - \mathbf{e_x}^\top \hat{\mathbf{J}}\mathbf{W}(\hat{\mathbf{J}}\mathbf{W})^\dagger \mathbf{K_x}\mathbf{e_x} \quad (22)$$

where $\dagger$ is the matrix pseudo-inverse, and $\mathbf{K_x}$ is the diagonal positive proportional gain matrix.

During position regulation, where $\dot{\mathbf{x}}_d = 0$,

$$\begin{aligned}\dot{V}(\mathbf{e_x}) &= \mathbf{e_x}^\top \hat{\mathbf{J}}\mathbf{W}(\hat{\mathbf{J}}\mathbf{W})^\dagger \mathbf{K_x}\mathbf{e_x} \\ &= \mathbf{e_x}^\top \hat{\mathbf{J}}\hat{\mathbf{J}}^\dagger \mathbf{K_x}\mathbf{e_x} \end{aligned} \quad (23)$$

For rank-deficient Jacobian estimates, $\text{rank}(\hat{\mathbf{J}}) = n$ and $\hat{\mathbf{J}}\hat{\mathbf{J}}^\dagger = \mathbf{I}$, then

$$\dot{V}(\mathbf{e_x}) = -\mathbf{e_x}^\top \mathbf{K_x}\mathbf{e_x} < 0. \quad (24)$$

for $\mathbf{K_x} > 0$, and is therefore asymptotically stable.

A similar proof can be shown that $\mathbf{e_F}$, when under force-setpoint control, $\dot{\mathbf{F}} = 0$, is stable when

$$\dot{V}(\mathbf{e_F}) = -{\mathbf{e_F}}^\top \mathbf{K}_r^{-1}\mathbf{K_F}\mathbf{e_F} < 0 \quad (25)$$

and since $\mathbf{K}_r^{-1}$ is the compliance of the system and is thus positive definite, then the condition holds that the system is asymptotically stable for $\mathbf{K}_r^{-1}\mathbf{K_F} > 0$, which is satisfied for the proportional gain $\mathbf{K_F} = k\mathbf{I}, k > 0$.

REFERENCES

[1] D. Trivedi, C. D. Rahn, W. M. Kier, and I. D. Walker, "Soft robotics: Biological inspiration, state of the art, and future research," Applied Bionics and Biomechanics, vol. 5, no. 3, pp. 99–117, 2008.

[2] L. S. Cowan and I. D. Walker, "The Importance of Continuous and Discrete Elements in Continuum Robots," International Journal of Advanced Robotic Systems, vol. 10, p. 1, 2013.

[3] M. C. Yip and D. B. Camarillo, "Model-less feedback control of continuum manipulators in unknown environments," IEEE Transactions on Robotics, vol. 30, no. 4.

[4] M. Mahvash and P. E. Dupont, "Stiffness Control of Surgical Continuum Manipulators," IEEE Transaction on Robotics, vol. 27, no. 2, pp. 334–345, 2011.

[5] A. Bajo and N. Simaan, "Hybrid motion/force control of multi-backbone continuum robots," The International Journal of Robotics Research, vol. 10.1177/02, 2015.

[6] I. A. Gravagne and I. D. Walker, "On the kinematics of remotely-actuated continuum robots," Robotics and Automation, no. April, pp. 2544–2550, 2000.

[7] I. A. Gravagne, C. D. Rahn, I. D. Walker, and S. Member, "Large Deflection Dynamics and Control for Planar Continuum Robots," IEEE/ASME Transactions on Mechatronics, vol. 8, no. 2, pp. 299–307, 2003.

[8] B. Jones and I. D. Walker, "Kinematics for multisection continuum robots," IEEE Transactions on Robotics, vol. 22, no. 1, pp. 43–55, 2006.

[9] S. Neppalli, M. a. Csencsits, B. a. Jones, and I. D. Walker, "Closed-Form Inverse Kinematics for Continuum Manipulators," Advanced Robotics, vol. 23, no. 15, pp. 2077–2091, 2009.

[10] R. Webster, J. Swensen, J. Romano, and N. Cowan, "Closed-form differential kinematics for concentric-tube continuum robots with application to visual servoing," Experimental Robotics, 2009.

[11] D. C. Rucker and R. J. Webster III, "Parsimonious evaluation of concentric-tube continuum robot equilibrium conformation." IEEE Transactions on Biomedical Engineering, vol. 56, no. 9, pp. 2308–11, 2009.

[12] P. Dupont, J. Lock, and B. Itkowitz, "Real-time Position Control of Concentric Tube Robots," IEEE International Conference on Robotics and Automation, pp. 562–568, 2010.

[13] P. E. Dupont, J. Lock, B. Itkowitz, and E. Butler, "Design and Control of Concentric-Tube Robots." IEEE Transaction on Robotics, vol. 26, no. 2, pp. 209–225, 2010.

[14] G. Chirikjian, "Conformational Modeling of Continuum Structures in Robotics and Structural Biology: A Review," Advanced Robotics, no. August 2015, pp. 1–13, 2015.

[15] D. B. Camarillo, C. F. Milne, C. R. Carlson, M. R. Zinn, and J. K. Salisbury, "Mechanics Modeling of Tendon-Driven Continuum Manipulators," IEEE Transactions on Robotics, vol. 24, no. 6, pp. 1262–1273, 2008.

[16] M. Ivanescu and V. Stoian, "A Variable Structure Controller for a Tentacle Manipulator," IEEE International Conference on Robotics and Automation, pp. 3155–3160, 1995.

[17] D. Trivedi, A. Lotfi, and C. Rahn, "Geometrically exact dynamic models for soft robotic manipulators," IEEE/RSJ International Conference on Intelligent Robots and Systems, vol. 24, no. 4, pp. 773–780, 2007.

[18] D. Braganza, D. M. Dawson, I. D. Walker, and N. Nath, "A neural network controller for continuum robots," IEEE Transaction on Robotics, vol. 23, pp. 1270–1277, 2007.

[19] R. J. Webster, J. M. Romano, and N. J. Cowan, "Mechanics of Precurved-Tube Continuum Robots," IEEE Transaction on Robotics, vol. 25, no. 1, pp. 67–78, 2009.

[20] J. Lock and P. E. Dupont, "Friction Modeling in Concentric Tube Robots," IEEE International Conference on Robotics and Automation, pp. 1139–1146, 2011.

[21] M. Ivanescu, N. Bizdoaca, and D. Pana, "Dynamic control for a tentacle manipulator with SMA actuators," IEEE International Conference on Robotics and Automation, pp. 2079–2084, 2003.

[22] J. Jayender, M. Azizian, and R. V. R. V. Patel, "Autonomous image-guided robot-assisted active catheter insertion," IEEE Transactions on Robotics, vol. 24, no. 4, pp. 858–871, 2008.

[23] K. Xu and N. Simaan, "An investigation of the intrinsic force sensing capabilities of continuum robots," IEEE Transactions on Robotics, vol. 24, no. 3, pp. 576–587, 2008.

[24] ——, "Analytic Formulation for Kinematics, Statics, and Shape Restoration of Multibackbone Continuum Robots Via Elliptic Integrals," Journal of Mechanisms and Robotics, vol. 2, no. 1, p. 011006, 2010.

[25] J. Jung, R. S. Penning, N. J. Ferrier, and M. R. Zinn, "A Modeling Approach for Continuum Robotic Manipulators: Effects of Nonlinear Internal Device Friction," IEEE/RSJ International Conference on Intelligent Robots and Systems, pp. 5139–5146, 2011.

[26] V. K. Chitrakaran, A. Behal, D. M. Dawson, and I. D. Walker, "Setpoint regulation of continuum robots using a fixed camera," Robotica, pp. 1504–1509, 2007.

[27] A. Reiter, A. Bajo, K. Iliopoulos, N. Simaan, and P. K. Allen, "Learning-Based Configuration Estimation of a Multi-Segment Continuum Robot," no. 2, 2012.

[28] R. J. Roesthuis, S. Janssen, and S. Misra, "On using an array of fiber Bragg grating sensors for closed-loop control of flexible minimally invasive surgical instruments," IEEE/RSJ International Conference on Intelligent Robots and Systems, pp. 2545–2551, 2013.

[29] S. C. Ryu and P. E. Dupont, "FBG-based shape sensing tubes for continuum robots," IEEE International Conference on Robotics and Automation, pp. 3531–3537, 2014.

[30] B. Kim, J. Ha, F. C. Park, and P. E. Dupont, "Optimizing curvature sensor placement for fast, accurate shape sensing of continuum robots," IEEE International Conference on Robotics and Automation, pp. 5374–5379, 2014.

[31] M. H. Raibert and J. J. Craig, "Hybrid Position/Force Control of Manipulators," Journal of Dynamic Systems, Measurement, and Control, vol. 103(2), no. June 1981, pp. 126–133, 1981.

[32] D. C. Rucker and R. J. Webster III, "Deflection-based force sensing for continuum robots: A probabilistic approach," IEEE/RSJ International Conference on Intelligent Robots and Systems, pp. 3764–3769, 2011.

[33] J. Mattingley and S. Boyd, "CVXGEN: A code generator for embedded convex optimization," Optimization and Engineering, vol. 13, no. 1, pp. 1–27, 2012.

[34] B. Siciliano and O. Khatib, Springer Handbook of Robotics. Springer, 2008.

[35] I. Mirsky and W. Parmley, "Assessment of passive elastic stiffness for isolated heart muscle and the intact heart," Circulation Research, vol. 33, no. 2, pp. 233–243, 1973.

[36] M. Martinek, C. Lemes, E. Sigmund, M. Derndorfer, J. Aichinger, S. Winter, H.-J. Nesser, and H. Pürerfellner, "Clinical impact of an open-irrigated radiofrequency catheter with direct force measurement on atrial fibrillation ablation." Pacing and Clinical Electrophysiology, vol. 35, no. 11, pp. 1312–8, 2012.